Solar Energy Materials 18 (1989) 299–313
North-Holland, Amsterdam

FORMATION OF SEMICONDUCTING IRON PYRITE BY SPRAY PYROLYSIS

G. SMESTAD

Hewlett-Packard Company, Optoelectronics Division, 370 West Trimble Road, San Jose, CA 95131, USA

A. DA SILVA

Universidade do Algarve, Ciencias Exactas, 8004 Faro Codex, Portugal

H. TRIBUTSCH, S. FIECHTER, M. KUNST, N. MEZIANI and M. BIRKHOLZ

Hahn-Meitner-Institut Berlin, Bereich Strahlenchemie, D-1000 Berlin 39, Germany

Received 21 November 1988

Conditions for the production of thin pyrite layers by spray pyrolysis have been investigated for potential use as a solar cell material. Best results were obtained from an aqueous molar ferric chloride to thiourea ratio of 0.03M:0.072M. The films were deposited on glass substrates at 350°C in presence of gaseous sulfur and were sprayed with nitrogen as carrier gas. A simple hydrolysis reaction mechanism is proposed where thiourea, iron chloride and sulfur react on the hot substrate to form CO_2, NH_3, HCl and FeS_2. The crystallinity and phase of the films was confirmed as pyrite by X-ray diffractometry. Steady state conductivity measurements showed the films to be extrinsic (self compensated) semiconductors with an activation energy of 0.03 eV. Steady state photoconductivity was negligible, although greater photoconductivity was found in Ru doped layers. Optical transmission measurements indicated a soft band edge due to grain boundaries. Non-contract time resolved microwave conductivity measurements were conducted to study the lifetime of photo-excited carriers. Only at high excitation intensities were reasonable carrier lifetimes detected. The film–substrate interface on the films showed a much higher recombination rate than the film–air interface. This effect can be explained by strain at the substrate–film interface. The films on glass substrates exhibited cracking pinholes that are believed to be due to the cooling action of the spray droplets and the differences in thermal expansion between pyrite and glass materials.

1. Introduction

Pyrite, FeS_2, is now of interest for solar energy conversion [1], as well as battery technology [2] and sulfide ore geochemistry [3]. Pyrite has been synthesized by MOCVD [1], chemical vapor transport [4], and evaporation [5]. To the synthesis methods can now be added a potentially inexpensive high volume processes for the production of pyrite films via chemical spray pyrolysis. Previous work done by Abass et al. [6,7] using this technique was confusing in the selection and valence of the iron salt used. The ratio of sulfur to iron species in the starting materials was

1:2 and not 2:1 as in pyrite. The optical band gap measured was also different than previous values for the materials [5,8]. For this reason, the present work was conducted to establish conditions and methods for spray deposition and to confirm and advance previous work. In the next sections will be elucidated the conditions for the production of semiconducting pyrite by spray pyrolysis and the characteristics of the films produced.

2. Experimental methods

The apparatus for the deposition of pyrite is shown in fig. 1. Glass substrates were held by a vacuum chuck connected to a water aspirator producing a vacuum ranging between 25 and 30 inch Hg. Glass for the deposition was 0.8 mm thick Corning 7059, 0.7 mm thick Schott AF45, or 0.19 mm thick Schott D263. The importance of the glass selection will be discussed shortly. The vacuum chuck was

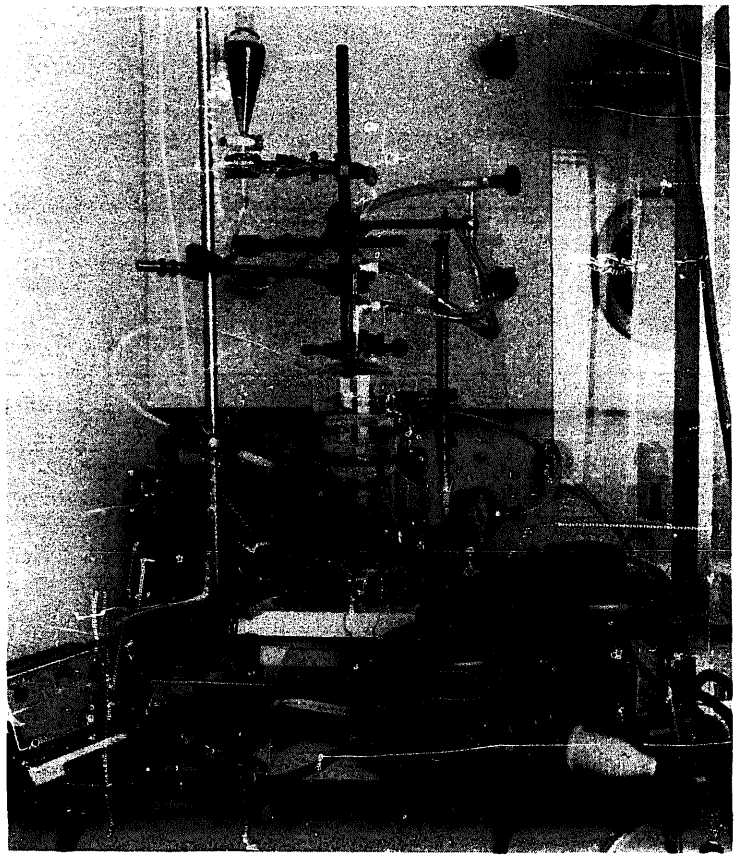

Fig. 1. A picture of the spray booth showing (from top to bottom) solution flask, spray nozzle, bell jar, vacuum chuck, and hot plate. Gases exit to the left of the vacuum chuck and a vacuum gauge is shown at lower right.

heated by a Thermolyne Cimerac hot plate and formed an isothermal reservoir for heat. This allowed the substrate to be uniformly maintained at the desired spray temperature. Temperature was controlled to within 5°C using an Omega 4001K

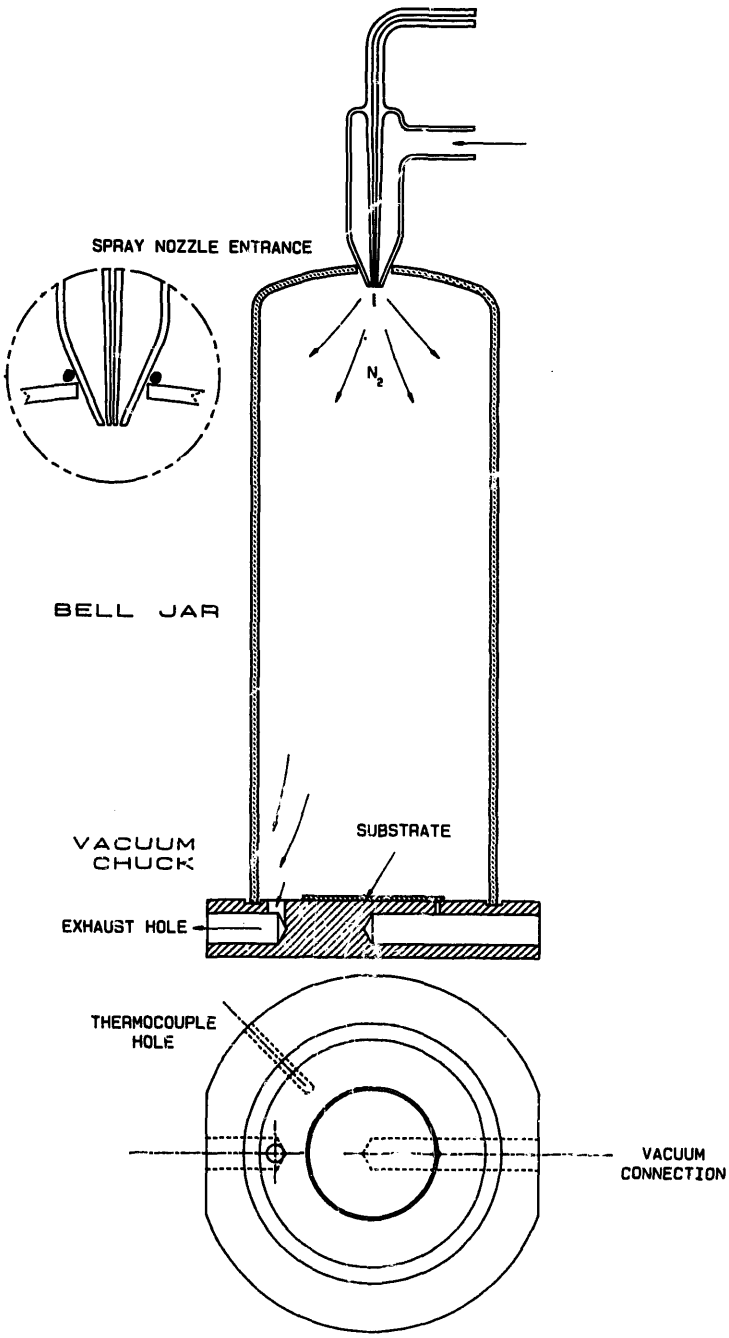

Fig. 2. Detailed diagram of the spray nozzle, bell jar and vacuum chuck showing the geometry and configuration used to deposited the films. The diagram is to scale with the substrate length of 5 cm. Above left is shown a detailed diagram of the spray nozzle entrance at expanded scale.

Table 1
The conditions for the preparation of semiconducting pyrite via spray pyrolysis (these conditions were used for the production of SP 7-28)

Flow of aqueous solution	1 mℓ/min
Flow of carrier gas	11 ℓ/min
Solution $FeCl_3$ concentration	0.03M
Thiourea : $FeCl_3$ ratio	2.24 : 1
Distance nozzle to substrate	23 cm
Temperature of chuck	350 °C
Chuck vacuum	−28 inch Hg
Film deposit seen in	<1 min
Total deposition time	10–40 min

temperature controller and checked using a Cole Parmer Key 9437-14 M surface probe thermometer. The control thermocouple was placed well within the isothermal vacuum chuck block. A flat bottom quartz bell jar was placed on the vacuum chuck in a round groove and thus isolated the film from the ambient air environment. The details of the vacuum chuck, spray nozzle and bell jar are shown in fig. 2. The spray nozzle was fabricated out of pyrex at SRI, but was similar to the commercially available 1/4 J SU-1 supplied by Spray Systems Corporation [9]. The spray nozzle entered the bell jar through an O-ring, which formed a seal. Reagent grade iron III chloride hexahydrate and thiourea was sprayed on the hot substrate using the spray nozzle. The solution was prepared in an electrochemical grade water solution ranging between 0.1M and 0.01M. Fresh solutions were prepared and mixed prior to each experimental spray run. The ratio of thiourea to $FeCl_3$ was greater than 2 : 1 in all experiments where pyrite was formed. The pH was measured between 2.0 and 2.5, depending on solution concentration. Gases produced exited along with the nitrogen carrier primarily through an exhaust (bubbler) outlet. Typical run conditions are shown in table 1. Approximately 1 g of free sulfur was added to the chamber in a small alumina boat placed on the heated vacuum chuck. During spraying, the evaporating sulfur coated the jar to decrease the oxygen partial pressure through the formation of SO_2 gas.

Films were characterized using a Phillips X-ray diffractometer. Phase identification was made from an analysis of intensity of the peak versus 2θ. Contacts were made to the films using Ag conductive paste. Steady state electrical measurements were taken via the constant voltage technique using a Keithley 619 electrometer and 230 voltage source [10]. Resistance was taken as a function of reciprocal temperature, for dark and light measurements. Time-resolved microwave conductivity measurements, TRMC, were conducted using the apparatus described in the literature [1]. The signals were induced using a 1 mJ/cm^2 Nd : YAG laser with a pulse width 20 ns at 532 and 1064 nm. These TRMC measurements were invaluable additions to the information provided by the constant voltage measurements, as they provided non-contact transient photoconductivity information.

3. Experimental results

3.1. General properties

All attempts to reproduce the conditions of Abass et al. resulted in Fe_2O_3 or oxide production using permutations of thiourea, $FeCl_3$, $FeCl_2$, air, and nitrogen. A summary of typical experimental runs is shown in table 2. This represents the most successful fraction of the experiments conducted via a statistically designed experimental process to explore optimum parameters. The film properties and characteristics are a strong function of pH, temperature, concentration, and nitrogen and solution spray rates. The results from a study of these parameters will appear in a subsequent paper. Films formed had wedge type character of increasing thickness with a maximum (center) value from 0.5 to 40 μm. They were opaque in transmission, shiny "gold black" in reflection. This appearance is in sharp contrast to previous pyrite spray work where transparent yellow films were reported [6,7]. Film SP 7-28 was characterized extensively, as it had the best properties without ruthenium addition.

3.2. Electrical properties

Microwave conductivity for this film excited from two different directions is shown in fig. 3a. The decay time, or 1/e falloff time, for the pyrite–air interface is approximately 5 μs, and is indicative of a material with reasonably long minority carrier lifetimes. The microwave photoconductivity of the pyrite–air interface of SP 7-28 was much better than of the pyrite-glass interface, which suggests lattice

Table 2
Summary of typical experimental runs showing characteristics of the films produced on various substrates (unless otherwise stated, the substrate material was D263) [a)]

SP run	$[Fe^{3+}]$	Temp	Liquid rate	Gas rate	Pinholes?	Phases	Comments
4-16 #2	0.1	350	1	15	Yes	Py, Mar	S^0 excess
7-26	0.1	350	1	15	Yes	Hem	O_2 used
7-27 #1	0.1	350	1	15	Yes	Py, Po	
7-28	0.03	350	1	11	Yes	Py, Mar?	
8-1	0.03	350	1	14	No	Py, Mag	Si sub
8-2	0.03	350	1	10	No	Py, Mar	Mo/glass
8-3	0.03	350	1	10	Yes	Py	Mica Sub
8-4 #1	0.03	350	1	10	No	Thin	Al Sub
8-5 #2	0.03	350	1	11	Few	Py	Ru added
8-16 I	0.03	315	0.5	15	Few	Py	
9-1	0.03	346	1.25	11	Yes	Py	7059 Sub
9-24 I	0.03	360	0.75	11	Few	Py	AF45 Sub
9-24 II	0.03	350	1	11	Few	Py	Ti/glass

[a)] *Py*: Pyrite FeS_2, *Hem*: hematite Fe_2O_3, *Mar*: marcasite FeS_2, *Mag*: maghemite Fe_3O_4, *Po*: pyrrhotite $Fe_{1-x}S$, *Sub*: substrate.

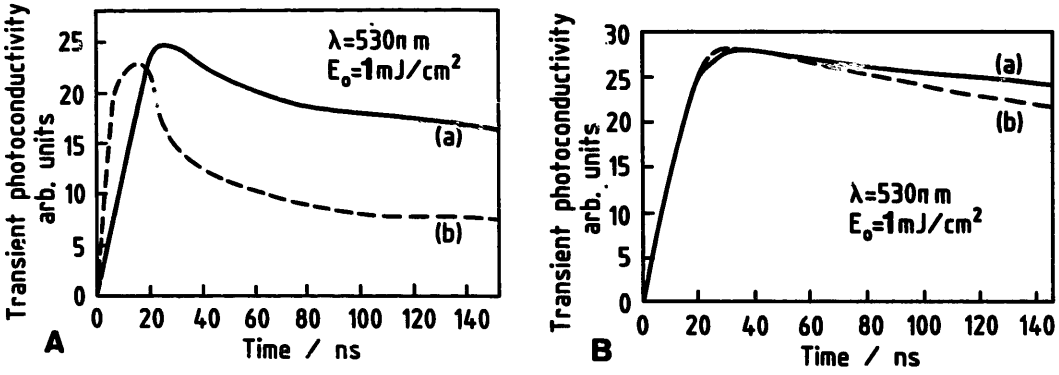

Fig. 3. (A) TRMC for SP 7-28 for: (a) pyrite-air interface, and (b) pyrite-glass interface; showing the large differences in recombination rate at the two interfaces. (B) TRMC for SP 8-5 for: (a) pyrite-air interface, and (b) pyrite-glass interface; showing the small differences in recombination rate at the two interfaces.

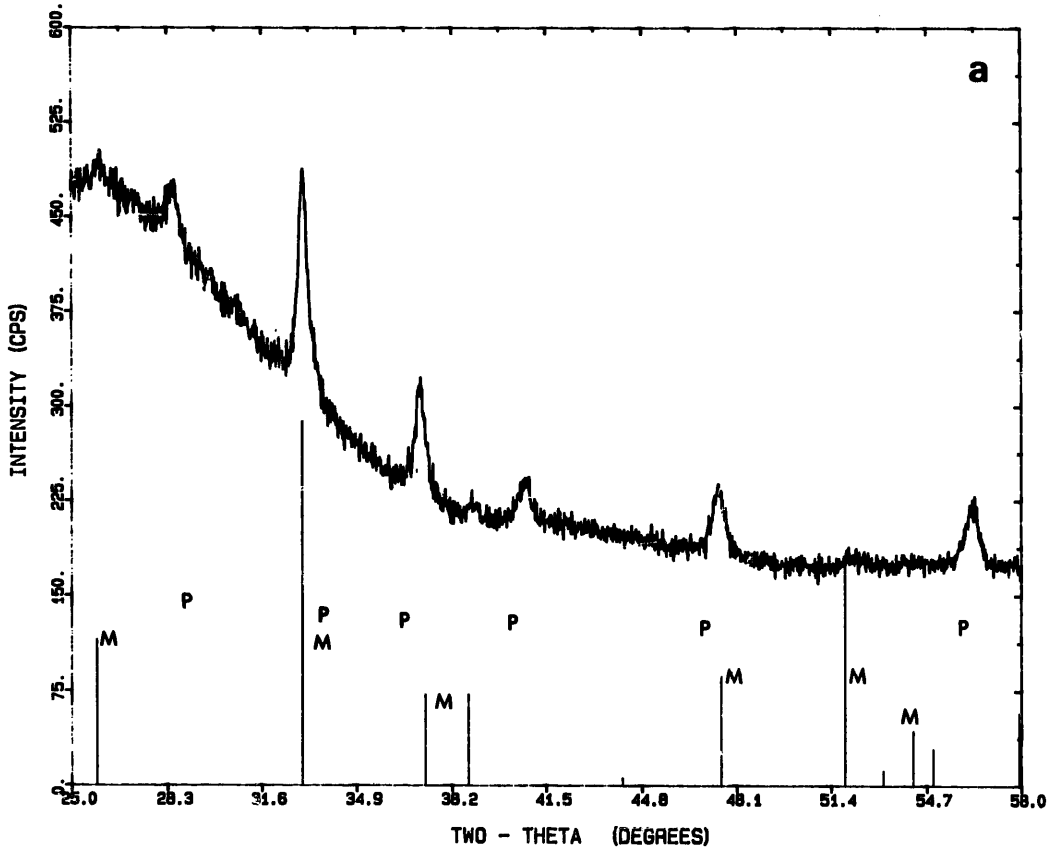

Fig. 4. X-ray diffraction for: (a) SP 7-28, and (b) SP 8-5. Shown as lines on the plots are the literature values for pyrite, marcasite and ruthenium disulfide.

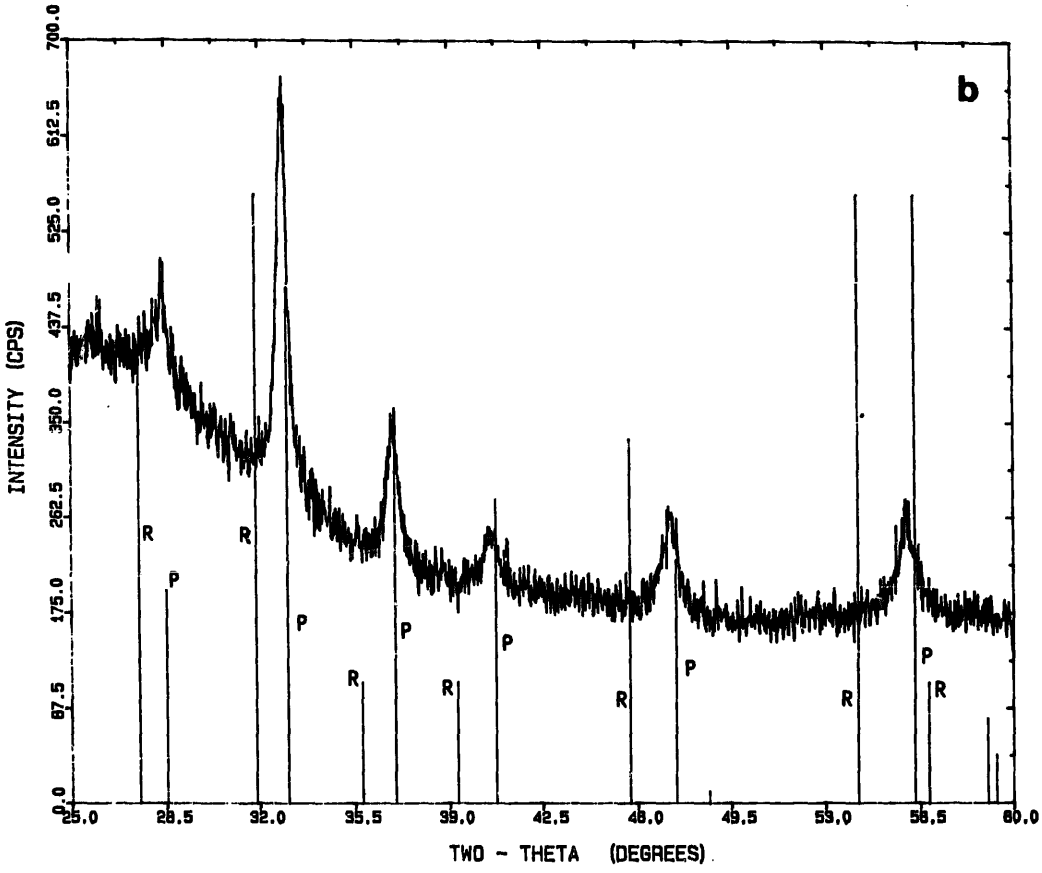

Fig. 4. Continued.

mismatch or strain at the substrate. For the longer wavelengths, which penetrated the material to a greater depth, this surface effect was observed to be greatly reduced. The steady state electrical properties showed a resistivity of 0.16 Ω cm, with an activation energy of 0.03 eV, determined from the temperature dependence of resistivity. A single slope, activation energy, was seen for the 333 to 128 K temperature ranged measured. The decrease in room temperature resistivity with the addition of light was less than 0.016%. Hall effect and Seebeck measurements indicated low mobility p-type material, although this observation must be reported cautiously, as the material could be heavily self-compensated. These observations can be explained by utilizing a mechanism of a barrier layer or impurities accumulated at grain boundaries or microscopic regions.

3.3. Phase analysis and compensation

To check for the presence of second phases, X-ray diffraction was done and is shown in fig. 4a. This shows the film to be single phase pyrite with possible trace marcasite. Films sprayed at a thiourea to Fe ratio of 4 : 1 at temperatures between 260 and 450 °C often contained much $Fe_{1-x}S$. It has suggested that when marcasite

is present over $Fe_{1-x}S$ increased sulfur incorporation has occurred [11]. EDAX measurements showed a sulfur to iron ratio of roughly 2:1, as well as no gross change in stoichiometry with position (K line area). Any barrier layers of the non impurity type are thus subtle. SEM photographs of this film shown in figs. 5a, 5b and 5c, show the columnar nature of the approximately 0.1–0.2 μm size grains. Shown in fig. 5a is a view of the pinholes present in the films. Grain size determined via the X-ray diffraction line broadening was approximately 1000 Å. This technique is described in ref. [1]. This is confirmed by the SEM photographs of fig. 5. EDAX

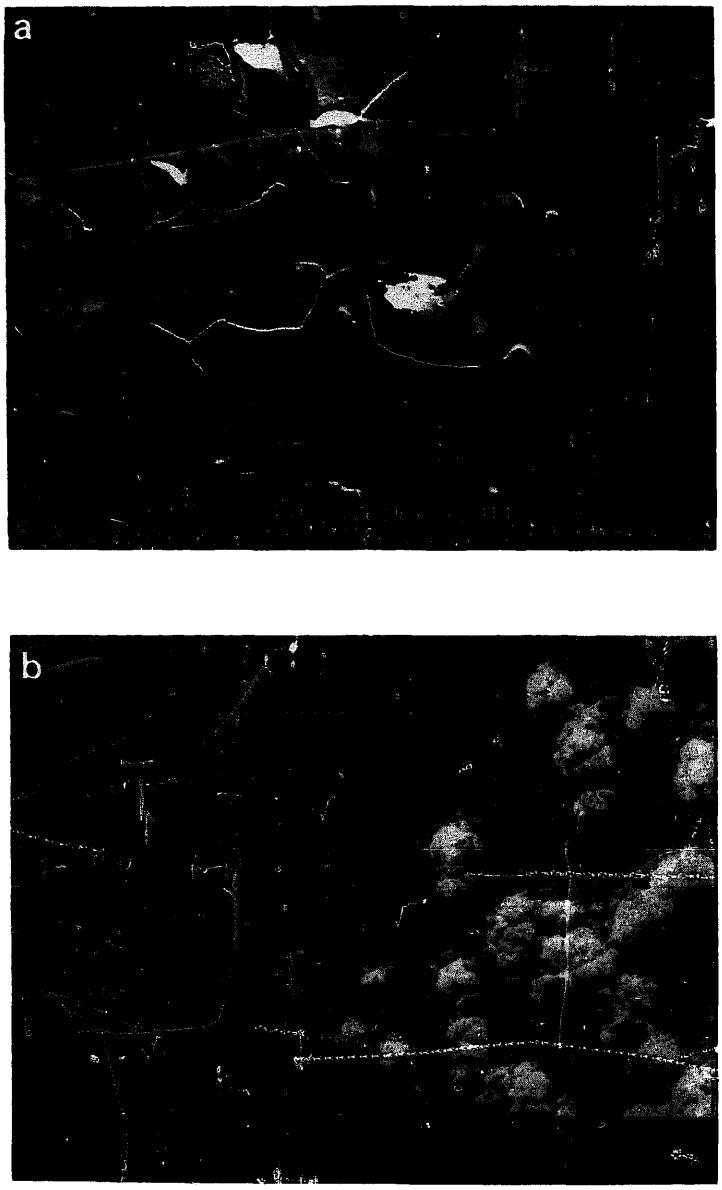

Fig. 5. Scanning electron micrographs for SP 7-28 showing (a) cracking pinholes, (b) 0.1 μm grains at higher magnification, and (c) side view of the film showing columnar grains and growth direction. Film thickness is approximately 2500 Å.

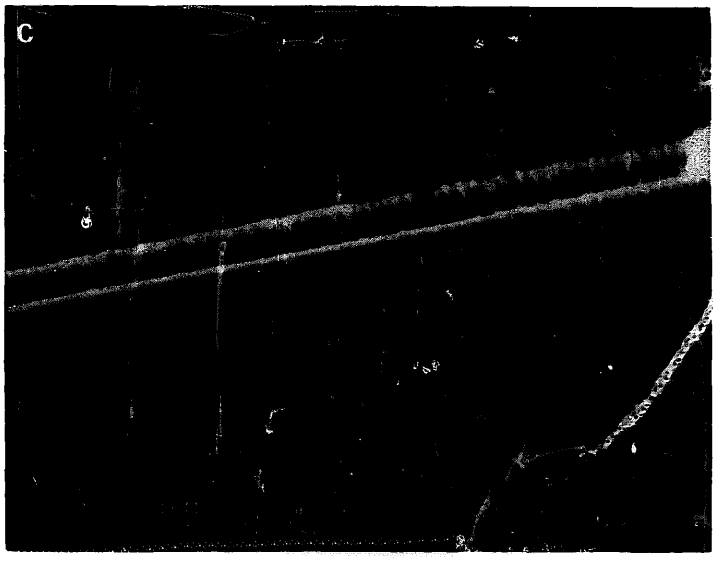

Fig. 5. Continued.

measurements of the areas with many pinholes showed Si, Na, K and Ti present in the D263 glass. Low level oxygen and carbon were detected in all areas. This was confirmed by Auger spectroscopy.

3.4. Optical properties

Optical measurements taken on a Bruins Omega 10 spectrophotometer of SP 7-28 are displayed in figs. 6a and 6b. The plot shows band edge softening characteristic of grain boundary states in polycrystalline material [12]. Also shown in fig. 6a at a wavelength of approximately 450 nm is a blue transmission that can also be observed when an incandescent light source is viewed through the film. Band gap determination is shown in fig. 6b using the procedure of Abass [7] and Sato [5]. This plot yields an indirect band gap of 0.82 eV, with a corresponding phonon energy of 0.06 eV. The optical absorption coefficient, α, at 850 nm was 1.6×10^5 cm^{-1} in good agreement with previous measurements [4,5].

3.5. Doping with ruthenium

Measurements of film SP 8-5 are shown in figs. 3b and 4b and show this ruthenium doped film to be of superior quality than the non-ruthenium doped counterpart SP 7-28. The ruthenium source was fresh $RuCl_3$ $3H_2O$, and was 0.004M in the final solution. The room temperature dark resistivity for this film was 0.13 Ω cm with an activation energy of 0.03 eV. This film exhibited a 0.03% decrease in resistivity upon illumination. A decrease in resistivity with temperature was observed for both SP 7-28 and SP 8-5, indicating semiconductor behavior.

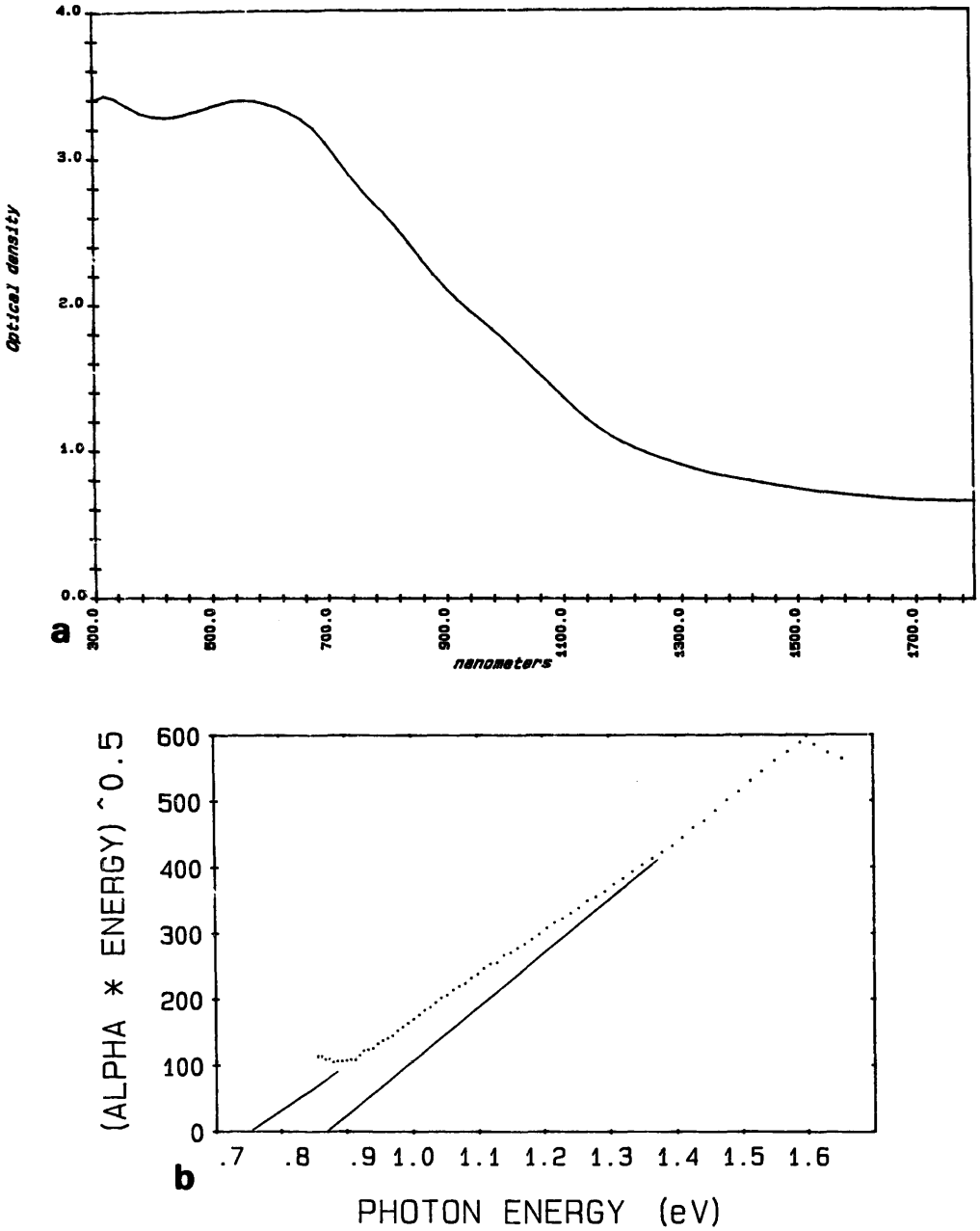

Fig. 6. Optical data: (a) optical density versus wavelength for the visible and near IR portion of the spectrum. Note the change in slope near 1150 nm. (b) $(\alpha h\nu)^{1/2}$ versus energy showing the indirect band gap and band edge softening.

4. Discussion

4.1. Film characteristics

There are two main problems to be solved regarding spray deposited pyrite before it can be used for solar cells. One is the problem of many pinholes which can

be seen in the SEM photograph of fig. 5a. The observation of the jagged nature of the holes, and of the material which is re-deposited in the holes, suggests that these are not non-adherence pinholes produced by material that is unable to stick to the glass. They seem to suggest a cracking mechanism. The mechanical strength of many glasses is improved by rapid cooling. This produces a region of permanent compression at the plate surface [13]. The cooling action of the spray droplets may then cause the stressed deposited material to flake off the substrate. Pyrite is a brittle material, and as such, axial cracking with dislocations have been observed for small grain material [14]. Most of the work done utilized 0.19 mm Schott D263 glass. Results on the other glasses showed similar cracking problems, although not as severe. The thermal expansion of the D263, AF45 and 7059 glasses, 7.3, 4.5, $4.6 \times 10^{-6}/°C$ respectively, may also play a role in the production of these cracking pinholes. Cracking problems have been noted for other brittle materials, such as $YBa_2Cu_3O_x$, using glass which is of low thermal expansion coefficient [15]. The thermal expansion of pyrite at $T = 0°C$ and 350°C is 8.4 and $13 \times 10^{-6}/°C$, respectively [16]. Note that for electrical and optical measurement purposes, small regions were taken from the perimeter of the 5 cm glass plate, as this region usually contained greatly reduced numbers of pinholes. The films sprayed at low rates or on metal/glass contained only few pinholes.

The other problem regarding the FeS_2 films deposited is electrical. Comparison of the results of TRMC with the photoconductivity at a steady state show an inconsistency to be explained. The films show photoconductivity in microwave but not in steady state measurements. One reason may be that the microwave measurements were done at 1 mJ/cm^2 at a duration of 20 ns (50×10^6 mW/cm^2). The steady state photoconductivity measurements were done at approximately 80 mW/cm^2. The microwave conductivity measurements were therefore done at conditions where one might expect traps and defects to be populated so that the material will behave more favorable to additional applied light. We do not believe that this is the only reason for the discrepancy. One should note that the slope of the $1/T$ plot, activation energy, was low and that the semiconductor's resistivity was also low. Similar effects were measured for film SP 8-2 both perpendicular and parallel to the film surface. One can postulate that there are barriers to photo-electron flow when a voltage is applied that are not traversed during the non-contact microwave measurements. During the microwave measurements the electron–hole pairs reside and recombine within a region of good photo properties. However, when a voltage is applied and these carriers are forced to traverse different material, they recombine and thus no photo signal from the excess charge carriers is seen. These recombination areas could reside in conductive $Fe_{1-x}S$ material. These pyrrhotite areas may be amorphous and would be undetected. One possible consequence of this may be that the material is FeS_{2-x}. It has been suggested that non-stoichiometry is a possible cause of a lower quality pyrite material, and that this can be partially alleviated by H insertion [17]. Attempts at duplicating the effects seen in ref. [17] resulted in the peeling of the films from the glass in the HI solution in most cases. As support for this non-stoichiometric theory, ruthenium was added to the film with the concurrent increase in photo properties. Ruthenium has to known monosulfide,

and as such, it was believed to favor a sulfur ratio of exactly 2:1. X-ray diffraction of SP 8-5 suggests a lattice parameter between FeS_2 and RuS_2, and thus a solid solution between Fe and Ru ($a_0(FeS_2) = 5.417$ Å, $a_0(RuS_2) = 5.57$ Å, a_0 from fig. 4b is 5.45 Å). Further work will be done to explore and confirm this mechanism.

A second possible cause could be impurities introduced by the glass. Schott D263 glass contains Na and K ions. These mobile ions may migrate into the film to destroy excess carrier lifetimes. Thus, experiments utilizing low alkali glasses 7059 and AF45 were done. The films produced on these glasses possessed similar electrical and photo effects. Films deposited on metals or metal-coated glass also mirrored the electrical results of the D263 glass.

The other substrate materials tried have not yet been optimized for the deposition of pyrite, as shown in table 2. The films on Al and Si were quite thin, perhaps due to the different emissivity and hence higher surface temperature and lower deposition efficiency. Films on Ti or Mo coated glass and mica were approximately as thick as those on glass alone. Further experiments can be done to optimize deposition on these materials by lowering the vacuum chuck and deposition temperatures.

As mentioned at the onset of this paper, the band gap measured for pyrite in previous spray work was not 0.9–0.95 eV, as in other pyrite work [4,6,7]. The bandgap determined in the present paper is 0.82 eV and is reasonably close to that of Sato [5] and Ennaoui [4]. Abass [6] is concerned with *forbidden* direct and indirect transitions, and as such, does not represent the optical band gap used in electrical or semiconductor junction devices. However, Abass [7] and Ennaoui or Sato [4,5] are in conflict as they report the indirect *allowed* optical band gap to be 1.25 and 0.95 eV, respectively. The discrepancy could be due to the transmission of the pyrite in the region of 0.9 to 1.3 μm, which shows considerable curvature and activity (see fig. 6 or ref. [4]). For pyrite as a d-type bonded rather than the usual s–p type bonded semiconductor, it may be necessary to modify the equations used to describe indirect transitions and optical absorption. This discrepancies in optical band gap in previous studies may also be due to Burstein shift due to the heavy doping present [18,12]. The possibility exists that the 1.25 eV valve is due partially to X-ray amorphous oxides or phases. Further work will be done to substantiate these explanations, however, there may always be problems when comparing fine grain polycrystalline to single crystal optical effects.

4.2. Chemistry

The mechanism for the production of dichalcogenide films by spray pyrolysis is believed to involve the hydrolysis of thiourea [19]. This mechanism has also been recently expanded to include the spray pyrolysis of $CuInSe_2$ [20,21]. The chemistry proposed for the production of pyrite by spray pyrolysis that is suggested involves: (1) the breakdown of hydrolysis of thiourea to hydrogen sulfide; (2) the reduction of Fe(III) to Fe(II) by hydrogen sulfide; (3) the reaction of Fe(II), hydrogen sulfide and sulfur to form pyrite. This hydrogen sulfide mechanism is also believed to occur in natural pyrite production [22,23].

The reaction sequence and balanced equation proposed is:

$$3\left[(NH_2)_2CS + 2\,H_2O + 2\,HCl \rightleftarrows CO_2 + 2\,NH_3 + 2\,HCl + H_2S\right]$$
$$\left[2\,FeCl_3 + H_2S \rightleftarrows 2\,FeCl_2 + S^0 + 2\,HCl\right]$$
$$2\left[x\,S^0 + H_2S \rightleftarrows 2\,H^+ + S_x^{2-}\right]$$
$$2\left[FeCl_2 + 2\,H^+ + S_x^{2-} \rightleftarrows FeS_2 + 2\,HCl + (x-2)\,S^0\right]$$
$$\overline{3\,(NH_2)_2CS + 6\,H_2O + 2\,FeCl_3 + S^0 \rightleftarrows 3\,CO_2 + 6\,NH_3 + 6\,HCl + 2\,FeS_2}$$

The Gibbs free energy for this reaction at 350 °C was calculated as −170 kcal/mol using the Gibbs–Heimholtz equation and assuming unit activity or molarity at the time of reaction [24]. The free sulfur in the equation can come from the added sulfur in the chamber, or most likely from the reaction of $H_2S + \frac{1}{2}O_2 \rightleftarrows H_2O + S^0$. Since H_2S can be produced from thiourea, this would bring the thiourea to Fe ratio to 2:1, as was used in the experiments. Note that Fe(III) is needed as an oxidizing agent to create polysulfide. The hydrolysis reaction may proceed via cyanamide to urea to CO_2 formation [19]. The production of sulfide was confirmed in the exit gases from the spray jar via the use of lead chloride containing paper (i.e. a dark spot of lead sulfide produced). The confirmation of CO_2 was made using a mass spectrometer analyzing the gases collected from the jar during spraying. Attempts using $FeCl_2$ resulted in $Fe_{1-x}S$ with FeS_2 production. This probably due to the fast kinetics of pyrrhotite over pyrite at high Fe^{2+} concentrations [22]. For a Fe(II)/thiourea reaction, Fe(III) would not be available to produce sulfur. Oxygen would then be needed to produce polysulfide, risking oxide formation. Comparison of runs SP 7-28 with SP 4-16 #2 and SP 7-27 #1 may yield insight into the reaction mechanism. Adding S^0 to the alumina boat seems to favor pyrite over pyrrhotite formation. This can be explained via the reaction mechanism, since sulfur favors polysulfide over sulfide formation [22]. Raising the solution concentration also favors pyrrhotite, again due to the fast kinetics of pyrrhotite over pyrite at high iron concentrations.

A competing reaction for the production of polysulfide from Fe(III) is the production of the oxidized thiourea dimer, formamidine disulfide, from Fe(III) [25]. This reaction can be seen to occur in 5 h aged solutions as a white precipitate. After 24 h, a yellow precipitate of sulfur is produced from the reaction of the excess thiourea or H_2S, with Fe(III) and oxygen. The Fe(II) concentration in the spray mixture was monitored as a function of time using Fe(II) sensitive paper. It was found that at $t = 0$, 19, 54 min the Fe^{2+} was 0, 300, 500 ppm, respectively. It is unknown as to importance of this reaction in pyrite formation, although it suggests that fresh solutions should be sprayed, or that the reactants should be mixed in situ. The redox potential of thiourea-formamidine disulfide system, +0.42 V, is between that of iron (II)/(III) and sulfide/sulfur. This would suggest that it could act as an intermediate or catalyst in the proposed reaction, being first oxidized by iron (III), then reduced back to thiourea by the sulfide produced by thiourea hydrolysis. As a further observation, mixing of the thiourea and $FeCl_3$ solutions creates a transient darkening to a brown solution that fades over 30 min to the color of the iron

solution alone. This could indicate a complex between thiourea and Fe(III) or the weak basic nature of the thiourea with the production of iron hydroxides [26]. Additional work will be done to substantiate these mechanisms as well as explore the relationship between stoichiometric material and deposition parameters.

5. Conclusions

Semiconducting pyrite has been produced by chemical spray pyrolysis. The method produces films at potential high volumes and the films can be configured on the glass plate as to take advantage of optical enhancement used for solar cells [27,28]. Although the films do not show strong photoconductivity at present, the material and deposition method warrants subsequent study. Further work needs to be done to establish the interaction between chemical mechanism, stoichiometry and photoelectrochemical properties. The focus of continuing work should be on the formation of the polysulfide needed for pyrite formation. Proper choice of, and metal coating for, the substrate material should also be explored further. With the completion of these studies "fool's gold" may finds its place in the sun.

Acknowledgements

We wish to express our gratitude to the Hahn-Meitner-Institute and DAAD for their support during this research. In particular, the assistance of Martin Wilhelm, Rolf Koenenkamp, Annita Irmscher, Paul Grunow, Sigrid Rumbaum, and Stefan Scholz was instrumental in this research. We would also like to thank Professor Dr. Clayton Bates, Jr. for the use of his facilities at Stanford University. Discussions with Brian Brown of Stanford University were also useful. We would also like to thank Kathi Cushman and Ban Poh Loh for the use of their graphics and editing skills.

References

[1] G. Chatzitheodorou and S. Fiechter, Mater. Res. Bull. 21 (1986) 1481.
[2] C.A. Vincent, Modern Batteries (Edward, London, 1982).
[3] M. Rodriguez-Leiva and H. Tributsch, Arch. Microbiol. 149 (1988) 401.
[4] A. Ennaoui and H. Tributsch, J. Electrochem Soc. 132 (1985) 1579.
[5] K. Sato, Progr. Crystal Growth Characterization 11 (1985) 109.
[6] A.K. Abass, J. Appl. Phys. 61 (1987) 2339.
[7] A.K. Abass, Phys. Status Solidi (a) 97 (1986) 243.
[8] A. Ennaoui and H. Tributsch, Solar Energy Mater. 14 (1986) 461.
[9] Spray Systems Co., Wheaton, IL 60188, USA (312) 665–5000.
[10] Automating High Resistance Measurements (Keithley Instruments, Inc., Cleveland, OH, 1984).
[11] D.W. Shoesmith, J. Electrochem. Soc. 126 (1979) 911.
[12] S. Fahrenbrunch and R. Bube, Fundamentals of Solar Cells (Academic Press, New York, 1983).

[13] Schott Technical Information, Technical Glasses Physical and Chemical Properties, Mainz, Fed. Rep. of Germany, 1982.
[14] K.R. McClay, Economic Geology 79, (1984) 400.
[15] R. Henry and H. Lessoff, J. Crystal Growth 85 (1987) 615.
[16] R.S. Krishnan, Thermal Expansion of Crystals (Pergamon, New York, 1973).
[17] N. Alonso-Vante, G. Chatzitheodorou, S. Fiechter, N. Mgoduka, I. Poulios and H. Tributsch, Solar Energy Mater. 18 (1988) 9.
[18] J. Pankove, Optical Processes in Semiconductors (Dover, New York, 1971).
[19] J. Mooney and S. Radding, Ann. Rev. Mater. Sci. 12 (1982) 81.
[20] B. Brown and C. Bates, J. Electrochem. Soc. 135 (1988) 1559.
[21] B. Haba and C. Bates, Thin Solid Films 158 (1988) 133.
[22] R. Howarth, Science 203 (1979) 49.
[23] D. Vaughan and J. Craig, Mineral Chemistry of Metal Sulfides (Cambridge University Press, Cambridge, 1978).
[24] I. Klotz, Chemical Thermodynamics (Benjamin/Cummings, Menlo Park, 1986).
[25] P.W. Preisler and L. Berger, J. Am. Chem. Soc. 69 (1947) 322.
[26] J.A. Dean, Ed., Lange's Handbook of Chemistry (McGraw-Hill, New York, 1970).
[27] B. Faughnan, J. Appl. Phys. 58 (1985) 2746.
[28] G. Smestad and P. Hamill, Appl. Opt. 23 (1984) 4394.